Vibrational dynamics of N–H, C–D, and C O modes in formamide

Jeong-Hyon Ha, Yung Sam Kim, and Robin M. Hochstrasser

Citation: The Journal of Chemical Physics **124**, 064508 (2006); doi: 10.1063/1.2162165

View online: http://dx.doi.org/10.1063/1.2162165

View Table of Contents: http://scitation.aip.org/content/aip/journal/jcp/124/6?ver=pdfcov

Published by the AIP Publishing

Vibrational dynamics of N–H, C–D, and C═O modes in formamide

Jeong-Hyon Ha, Yung Sam Kim, and Robin M. Hochstrasser[a)]
Department of Chemistry, University of Pennsylvania, Philadelphia, Pennsylvania 19104

(Received 2 November 2005; accepted 5 December 2005; published online 14 February 2006)

By means of heterodyned two-dimensional IR photon echo experiments on liquid formamide and isotopomers the vibrational frequency dynamics of the N–H stretch mode, the C–D mode, and the C═O mode were obtained. In each case the vibrational frequency correlation function is fitted to three exponentials representing ultrafast (few femtoseconds), intermediate (hundreds of femtoseconds), and slow (many picoseconds) correlation times. In the case of N–H there is a significant underdamped contribution to the correlation decay that was not seen in previous experiments and is attributed to hydrogen-bond librational modes. This underdamped motion is not seen in the C–D or C═O correlation functions. The motions probed by the C–D bond are generally faster than those seen by N–H and C═O, indicating that the environment of C–D interchanges more rapidly, consistent with a weaker C–D···O═C bond. The correlation decays of N–H and C═O are similar, consistent with both being involved in strong H bonding. © *2006 American Institute of Physics*. [DOI: 10.1063/1.2162165]

I. INTRODUCTION

Interactions and angular relationships between vibrators and the dynamics of their frequency fluctuations can be measured by multidimensional IR spectroscopy.[1–4] The frequency bandwidth of the excitation infrared pulses is controlled to span the distribution of interacting states in these experiments. The heterodyned two-dimensional (2D) IR spectroscopy has now been applied to the measurement of structures and dynamics of various peptides and proteins.[5–7] These systems have repeating units giving rise to sets of nearly degenerate vibrations. Similar situations in solids, liquids, or glasses are encountered where the vibrational states of different molecules couple together to form excitation bands. Therefore, the heterodyned 2D IR spectroscopy also can help visualize the structure and dynamics of liquids.[8–12] Although the conventional Fourier transform infrared (FTIR), stationary and time-resolved nonlinear Raman methods, and other forms of ultrafast vibrational spectroscopy have had many applications to liquids and have contributed substantially to the understanding of liquid state dynamics, the method of 2D IR heterodyned echo spectroscopy used in this paper is an interesting complement to these approaches.[13] Here, we discuss experiments using the ultrafast heterodyned 2D IR to examine the H-bonded liquid, formamide.

Formamide is the smallest unit in a peptide chain and forms extended hydrogen-bond networks in its liquid state.[14–18] The intramolecular hydrogen bonds formed by peptides determine the secondary structures of protein; so from this standpoint liquid formamide is particularly interesting.[19] It has four different types of chemical bonds whose dynamical properties can be accessed by nonlinear infrared studies of its IR active modes. In a previous experiment, we probed the dynamics and motions of N–H bond in formamide. Excitation of the N–H mode induces relaxation into low-frequency modes of the liquid.[10] This relaxation causes distinctive signals in 2D IR photon echo experiments that permit measurement of the correlation of the frequency distributions of the N–H mode and the modes to which it transfers energy. These modes were found to be strongly correlated. Since the N–H mode distribution width is largely determined by H-bonding strength, with weak H bonds giving higher-frequency transitions, the relaxed modes were presumed to have the same characteristic. Librations and stretching of H-bonded molecules were reasonable candidates to account for the observed strong correlation. However, the fastest component of frequency correlation function was not fully explored in these experiments. Therefore, we have conducted a more extensive study of this short-time regime. The C–H or C–D mode is expected to be involved in the hydrogen-bonding network and it was thought that its dynamics might provide a more detailed picture of the liquid formamide structure. To the best of our knowledge, there are no previous reports of the ultrafast nonlinear IR photon echo of a C–D mode. The C–D transition lies in the 1800–2600 cm^{-1} region where there are few interferences from other modes even in proteins.[20–23] Through the C–D mode, the role of the CD···O hydrogen bonding in the overall structure and dynamics of formamide can be examined. This type of hydrogen bond is a weak attractive interaction whose existence has been experimentally predicted and demonstrated both by spectroscopic and crystallographic techniques.[24–28] Recently, the possible importance of the CH···O hydrogen bonding in the dynamics and structures of membrane proteins has been recognized.[29,30] The amide-I (carbonyl stretch) is one of the major IR active modes in formamide liquid structure.[31,32] This mode is involved in the extended hydrogen-bonding network and, therefore, its behavior is expected to be highly correlated with other modes in liquid formamide.

[a)]Electronic mail: hochstra@sas.upenn.edu

The present work examines the equilibrium dynamics of the N–H stretching, C–D stretching, and C═O stretching motions of liquid formamide. Their frequency correlation functions were compared in order to find an improved experimental description of the immediate environment to which each of these modes is coupled in the liquid.

II. EXPERIMENT

A. Sample preparation

1. DCONHD in deuterated formamide ($DCOND_2$)

The sample (2% DCONHD) was made by fully mixing the formamide-H_3 with liquid deuterated formamide-D_3. Both reagents were from Aldrich. The FTIR absorption spectra were obtained at 1 cm^{-1} resolution. The sample optical density for the echo experiments at the peak was ~0.3 in a CaF_2 cell of path length of 12 μm.

2. $DCONH_2$ in formamide ($HCONH_2$)

This sample (8% $DCONH_2$) was prepared by mixing the liquids formamide-D_3 and formamide-H_3. The optical density in the echo experiment was ~0.15 in a path length of 25 μm. The integrated absorption cross section of the C–D mode was 16% larger for this sample than formamide-D_3 in $CHCl_3$.

3. $HCONH_2$ in bulk formamide

A thin film of pure $HCONH_2$ having an optical density of ~0.1 at the carbonyl peak was prepared by spreading the liquid formamide between CaF_2 windows.

B. Laser instrument and signal definitions

1. 3 μm region experiment

The experiments were performed with the same instruments and methods reported previously.[10] Briefly, the pulses in the 3 μm region were generated by a Ti:sapphire regenerative amplifier (Spectra Physics Spitfire) and a homemade IR optical parametric amplifier (OPA).[33] The resulting 3.5 μJ pulses of duration ~75 fs had a full spectral width at half maximum of 190 cm^{-1} and were centered at 3.3 μm (3335 cm^{-1}). The IR pulse was divided into three excitation beams (k_1,k_2,k_3) that generated the IR echo. A weak local oscillator beam (k_{LO}) heterodyned the generated echo field and was sent to a monochromator having a liquid-N_2-cooled 32-element mercury cadmium telluride (MCT) array detector at the focal plane. The local oscillator beam and echo signals were separated by 500 fs to facilitate the spectral resolution and data processing. The heterodyned IR photon echo signal was measured as a function of the frequency ω_t detected at 32 discrete wavelengths, the time interval between the first and second pulses, τ, and the time interval between second and third pulses, T. The echoes directed into $-k_1+k_2+k_3$ with k_1 arriving at the sample before/after k_2 are referred to as rephasing/nonrephasing types for which we use the symbols R/NR. We obtained the three-time signal $S(\tau,T,t)$ by numerical Fourier transformation on the monochromator frequency axis. The inverse Fourier transformation on the t axis of $S(\tau,T,t)$ defines $\tilde{S}(\tau,T,\omega_t)$. A numerical Fourier transformation of $\tilde{S}(\tau,T,\omega_t)$ on the τ axis generated the complex 2D IR spectra, $\underline{S}(\omega_\tau,T,\omega_t)$. The real parts of the projections can be obtained by taking discrete sums over the ω_τ data sets $[\Sigma_{\omega_\tau}\underline{S}_R(\omega_\tau,T,\omega_t)e^{i\phi_R}$ and $\Sigma_{\omega_\tau}\underline{S}_{NR}(\omega_\tau,T,\omega_t)e^{i\phi_{NR}}]$. These projections reproduce the measured pump/probe spectrum at T, defined as $\tilde{S}(\tau=0,T,\omega_t)$ by adjusting the phases ϕ_R and ϕ_{NR} to find the best agreement. With the proper phases included the sum of the rephasing and nonrephasing signals generates a pure 2D IR absorptive spectrum, or more simply 2D IR spectrum. A profile along τ at each detection frequency ω_t can be obtained from each of the multidimensional data sets, such as $|\tilde{S}(\tau,T,\omega_t)|$. This function gives a complete set of T-dependent data at each ω_t, which is similar to that obtained from the stimulated three-pulse photon echo signal. We characterize each profile by the value of τ at which it has a maximum: the so-called peak shift.

2. 5–6 μm region experiment

Fourier-transform-limited 80 fs pulses with center frequencies 2169 and 1685 cm^{-1} were used in the 2D IR experiments. Three 400 nJ IR pulses with wave vectors k_1, k_2, and k_3 were incident on the sample, and the phase-matched signal at wave vector $-k_1+k_2+k_3$ was detected by heterodyning it with a local oscillator pulse that always preceded the signal pulse by a fixed interval of ~1.0 ps. The signal and local oscillator pulses were combined at the focal plane of a monochromator having a 64-element MCT array detector (IR Associates, Inc.). Each detector element is 200 μm in width and 1 mm in height. The focal length of the monochromator is 270 mm and the groove density of the grating used in our experiments was 50 lines/mm. The raw data collected using this method were in the form of a two-dimensional array of time τ, in 2 fs steps from −2.0 to 2.0 ps, and wavelength in ~6 nm steps. The procedures to obtain 2D IR absorptive spectra and peak shift profile were as described above.

In all experiments there were nonresonant background signals that could be seen when the pulse center frequency was not centered on a transition. However, the resonant signal completely dominated the nonresonant signal in all cases.

III. RESULTS

A. DCONHD in deuterated formamide ($DCOND_2$)

The linear IR spectrum (solid line) of 2% DCONHD in deuterated formamide, $DCOND_2$, in the N–H stretch vibration region is shown in Fig. 1. The broad featureless background coming from fully deuterated formamide is removed from the measured linear IR-absorption spectrum. The N–H band position is shifted to a frequency that indicates that the N–H groups are hydrogen bonded. The IR pulses have sufficient bandwidth to span the fundamental $0\rightarrow1$ transition as shown in Fig. 1.

From the heterodyned 2D IR signals, we can obtain the magnitude of $|\tilde{S}(\tau,T,\omega_t)|$ by Fourier transforming the three-time photon echo signal along the t axis. The profile of the quantity $|\tilde{S}(\tau,T,\omega_t)|$ vs τ is peaked at finite values of τ for each value of T. The peak shifts in Fig. 2 were obtained from the sums of $|\tilde{S}(\tau,T,\omega_t)|$ over ω_t from 3277 to 3357 cm^{-1} for

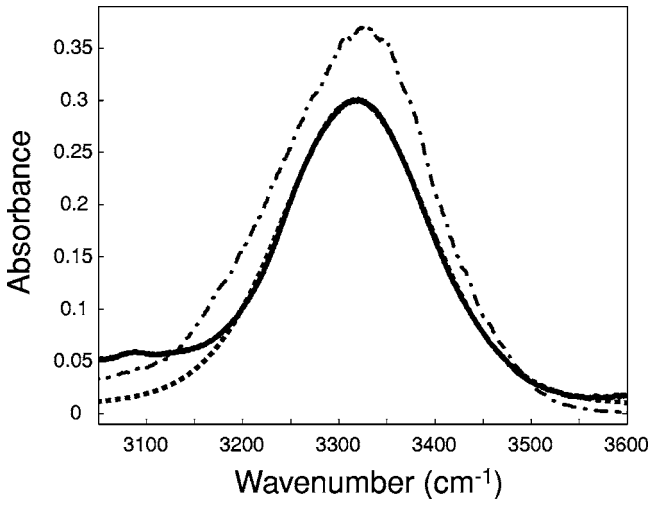

FIG. 1. Linear IR-absorption spectrum (solid line) of the N–H stretch vibration of DCONHD in formamide-D_3. The dotted line shows the spectrum obtained by Fourier transformation of the response function [Eq. (17)]. The dash-dot line indicates the laser-pulse spectrum.

each τ value. The center frequency of the signal $|\tilde{S}(\tau,T,\omega_t)|$ along ω_t is at 3317 cm^{-1}, which is at the peak of the fundamental transition. The peak shift decays after $T=0$ and it exhibits a damped oscillation that increased the peak shift to a maximum at $T=160$ fs after which it decayed, as shown in Fig. 2.

We simulated the linear spectrum and the peak shift profile with the methods reported previously,[10] and summarized again here, in which the photon echo response functions consist of a set of eight Liouville pathways. Four of these pathways describe the rephasing and the other four describe the nonrephasing contributions. The excited-state and ground-state population gratings contribute four pathways. Included also are the two pathways involving $\nu=1$ to $\nu=2$ transitions. The T_1 relaxation of the $\nu=1$ excitation of N–H populates other unknown vibrational states of the system,[10] which we symbolized by $|y\rangle$. We showed that these $|y\rangle$ states probably involve relative motion of formamide molecules. Two pathways are included that involve the excitation ($\nu=0\rightarrow\nu=1$) of N–H modes when the system is in the $|y\rangle$ states. In the simulations, the response functions can be written in terms of the four relaxation functions G:

$$G_{xx}^{R}(\tau,T,t) = -g_{xx}(\tau) + g_{xx}(T) - g_{xx}(t) - g_{xx}(T+\tau) - g_{xx}(t+T) + g_{xx}(\tau+T+t), \quad (1)$$

$$G_{xy}^{R}(\tau,T,t) = -g_{xx}(\tau) + g_{xy}(T) - g_{yy}(t) - g_{xy}(T+\tau) - g_{xy}(t+T) + g_{xy}(\tau+T+t), \quad (2)$$

$$G_{xx}^{NR}(\tau,T,t) = -g_{xx}(\tau) - g_{xx}(T) - g_{xx}(t) + g_{xx}(T+\tau) + g_{xx}(t+T) - g_{xx}(\tau+T+t), \quad (3)$$

$$G_{xy}^{NR}(\tau,T,t) = -g_{xx}(\tau) - g_{xy}(T) - g_{yy}(t) + g_{xy}(T+\tau) + g_{xy}(t+T) - g_{xy}(\tau+T+t). \quad (4)$$

The simplest forms for the relevant responses R_1 through R_8, neglecting coherence transfer, involve the fundamental frequencies ω_{10}, the anharmonicity Δ, the foregoing G factors, and the conditional probability factors, as follows:

$$R_1 = P(1,0|1,T)e^{-i\omega_{10}(t-\tau)}e^{G_{xx}^{R}(\tau,T,t)}, \quad (5)$$

$$R_2 = P(0,0|0,T)e^{-i\omega_{10}(t-\tau)}e^{G_{xx}^{R}(\tau,T,t)}, \quad (6)$$

$$R_3 = -2P(1,0|1,T)e^{-\alpha t/T_1}e^{-i((\omega_{10}-\Delta)t-\omega_{10}\tau)}e^{G_{xx}^{R}(\tau,T,t)}, \quad (7)$$

$$R_4 = -\sum_y P(1,0|y,T)e^{-i((\omega_{10}-\Delta_y)t-\omega_{10}\tau)}e^{G_{xy}^{R}(\tau,T,t)}, \quad (8)$$

$$R_5 = P(1,0|1,T)e^{-i\omega_{10}(t+\tau)}e^{G_{xx}^{NR}(\tau,T,t)}, \quad (9)$$

$$R_6 = P(0,0|0,T)e^{-i\omega_{10}(t+\tau)}e^{G_{xx}^{NR}(\tau,T,t)}, \quad (10)$$

$$R_7 = -2P(1,0|1,T)e^{-\alpha t/T_1}e^{-i((\omega_{10}-\Delta)t+\omega_{10}\tau)}e^{G_{xx}^{NR}(\tau,T,t)}, \quad (11)$$

$$R_8 = -\sum_y P(1,0|y,T)e^{-i((\omega_{10}-\Delta_y)t+\omega_{10}\tau)}e^{G_{xy}^{NR}(\tau,T,t)}. \quad (12)$$

The relevant transition dipoles, not shown explicitly in the equations, are assumed to be constants obeying $\mu_{21}^2=2\mu_{10}^2$. This harmonic approximation is consistent with the nearly equal relative intensities of the two peaks in the pump-probe spectra for all the modes. The value of μ_{10}^2 was taken as unity in the expressions for the responses. The R_3 and R_7 diagrams contain an additional $e^{-\alpha t/T_1}$ term to account for the faster relaxation of the $\nu=2$ compared with the $\nu=1$ level. For a harmonic oscillator α would be unity. The factors $P(\nu,0|\nu',b)$ represent the conditional probabilities that given a molecule is in the population state with quantum number ν of the mode at time 0 it will be in a state $|\nu'\rangle$ at time b. These factors may be calculated from the kinetics of the multiple level system. Each R describes the contribution to the signal from the evolution occurring in a particular subensemble of the molecules. The probability $P(0,0|0,T)$ is taken to be unity. Vibrational energy relaxation T_1 is taken

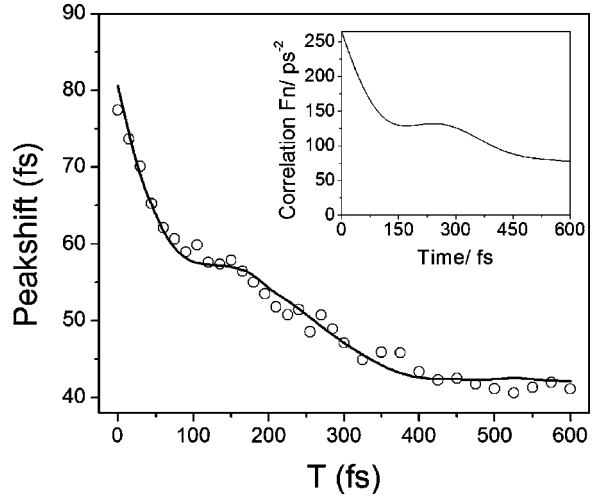

FIG. 2. The measured (circle) and simulated (solid line) peak shifts of the spectrally resolved echo of the N–H stretch vibration as a function of waiting time T. The inset shows the vibrational frequency correlation function.

into account through the multiplication factors, $\exp(-(\tau+t)/2T_1)$. In the vibrational relaxation process other internal and intermolecular modes may become excited. While the primary modes in the relaxation pathway would be those that are strongly anharmonically coupled to the mode being considered, some of these accepting modes may pass on their energy to more weakly coupled modes during the experimental time scale. For the case of N–H only we assume, as in previous work,[10] that levels $|y\rangle$ are excited by relaxation of the $\nu=1$ state. The $|y\rangle$ states do not have any N–H excitation but they may be excited to levels $|y+1\rangle$ by infrared pulses in the range of 3 μm corresponding to the addition of one quantum of N–H excitation. Possibly there are many states involved in the relaxation, but they are modeled by two response functions R_4 and R_8. As before[10] the state(s) $|y\rangle$ are assumed to have similar anharmonicity $\bar{\Delta}$, and therefore

$$\sum_y P(10|yT)e^{i\Delta_y t} = (1-e^{-T/T_1})e^{i\bar{\Delta}t}. \tag{13}$$

In the responses the fluctuations in the mode frequency are labeled as $x(t)$ while the y-state fluctuations are labeled as y. The real part of the line-shape function $g(t)$ is then defined as

$$g_{xy}(t) = \int_0^t d\tau_1 \int_0^{\tau_1} d\tau_2 \langle x(\tau_2)y(0)\rangle, \tag{14}$$

which is symmetric in x and y. The fluctuations in ω_{10} and ω_{21} are assumed to be strictly correlated so the same parameters were used in g_{xx} for both the $\nu=0\rightarrow\nu=1$ and the $\nu=1\rightarrow\nu=2$ transitions. The parameters in g_{yy}, which describe the N–H mode dynamics when it is associated with a mode $|y\rangle$, are the same as those in g_{xx}. It was shown previously[10] that frequency fluctuations of the N–H and the $|y\rangle$ modes are correlated with a correlation coefficient of 0.51. The third-order real three-time electric field signal was simulated by convolution of the response functions R_j with the electric fields of the laser pulses:

$$\begin{aligned} S(\tau,T,t) = \mathrm{Re}\Bigg\{ & \int_{-\infty}^{\infty} dt_1 \int_{-\infty}^{\infty} dt_2 \int_{-\infty}^{\infty} dt_3 \sum_j R_j(t_1,t_2,t_3) \\ & \times E_3(t-t_3)e^{-i\omega(t-t_3)} \\ & \times E_2(t+T-t_3-t_2)e^{-i\omega(t+T-t_3-t_2)} \\ & \times E_1(t+T+\tau-t_3-t_2-t_1)e^{-i\omega(t+T+\tau-t_3-t_2-t_1)} \Bigg\}. \end{aligned} \tag{15}$$

The response functions R_j's in the simulation incorporated all time orderings that could arise from pulses of duration of 75 fs.

The vibrational frequency correlation function of the N–H mode is described by the following fitting function with 14 parameters:

$$\begin{aligned} \langle x(t)x(0)\rangle = & a_1^2 \exp(-t/t_1) + a_2^2 \exp(-t/t_2) \\ & + a_3^2 \exp(-t/t_3) + a_4^2 \exp(-t/\tau_1)\cos(\omega_1 t + \phi_1) \\ & + a_5^2 \exp(-t/\tau_2)\cos(\omega_2 t + \phi_2). \end{aligned} \tag{16}$$

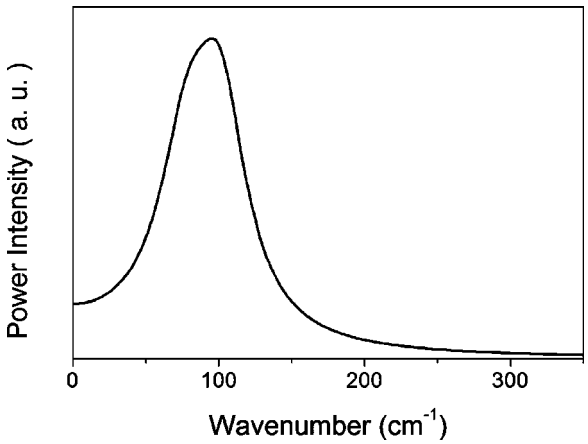

FIG. 3. The power spectrum of the frequency correlation function of the sum of the two underdamped oscillatory components of N–H.

The sum of oscillatory terms (two damped cosine functions) is incorporated because the peak shift profile shows oscillations around $T=160$ fs, which means that the correlation function of the N–H frequency must contain an underdamped oscillation. With these correlation functions and knowing that the overall rotational motion makes a negligible contribution,[10] the linear spectrum was simulated by Fourier transformation of the linear response function:

$$R_{linear} = e^{-g(t)-i\omega_{10}t-t/2T_1}. \tag{17}$$

As shown in Fig. 1, the simulation agrees well with experiments except for the small deviation at lower frequency. The absolute magnitude quantity $|\tilde{S}_R(\tau,T,\omega_t)|$ was obtained from the Fourier transform of the third-order real three-time electric-field signal and used to simulate and fit the peak shifts for a set of T values. The best-fit set of 14 parameters in the correlation function which satisfy both the linear spectrum and peak shift profile were found to be $a_1=10$ ps^{-1}, $a_2=6.1$ ps^{-1}, $a_3=9.9$ ps^{-1}, $a_4=4.9$ ps^{-1}, $a_5=4.9$ ps^{-1}, $t_1=0.15$ ps, $t_2=0.86$ ps, $t_3=11$ ps, $\tau_1=0.23$ ps, $\tau_2=0.25$ ps, $\omega_1=80$ cm^{-1}, $\omega_2=100$ cm^{-1}, $\phi_1=1.0$, and $\phi_2=0.85$. This correlation function, shown as an inset in Fig. 2, exhibits a peak at 240 fs and requires a phase shift. Among the three exponential components, the time constant of the fastest part is much faster than the estimates based on the many fewer data points of the previous experiment. The oscillation around $T=240$ fs was not definitively captured in the earlier report although it was the hint of these oscillations from a few data points that led to the present study. The oscillatory feature is well represented by the sum of the two damped cosine functions having similar amplitudes and damping time constants.

The power spectrum of the Fourier transform of the sum of the oscillatory parts is shown in Fig. 3. A power spectrum peaking at $\sim$95 cm^{-1} is consistent with the results from far-infrared absorption,[34] optical-heterodyne-detected Raman-induced Kerr effect spectroscopy (OHD-RIKES),[35–37] and depolarized Rayleigh/Raman spectroscopy.[38,39] In these experiments peaks at $\sim$100 and $\sim$190 cm^{-1} were observed and assigned as hydrogen-bond librational motional modes. The low-frequency vibrational mode near $\sim$100 cm^{-1} appears to

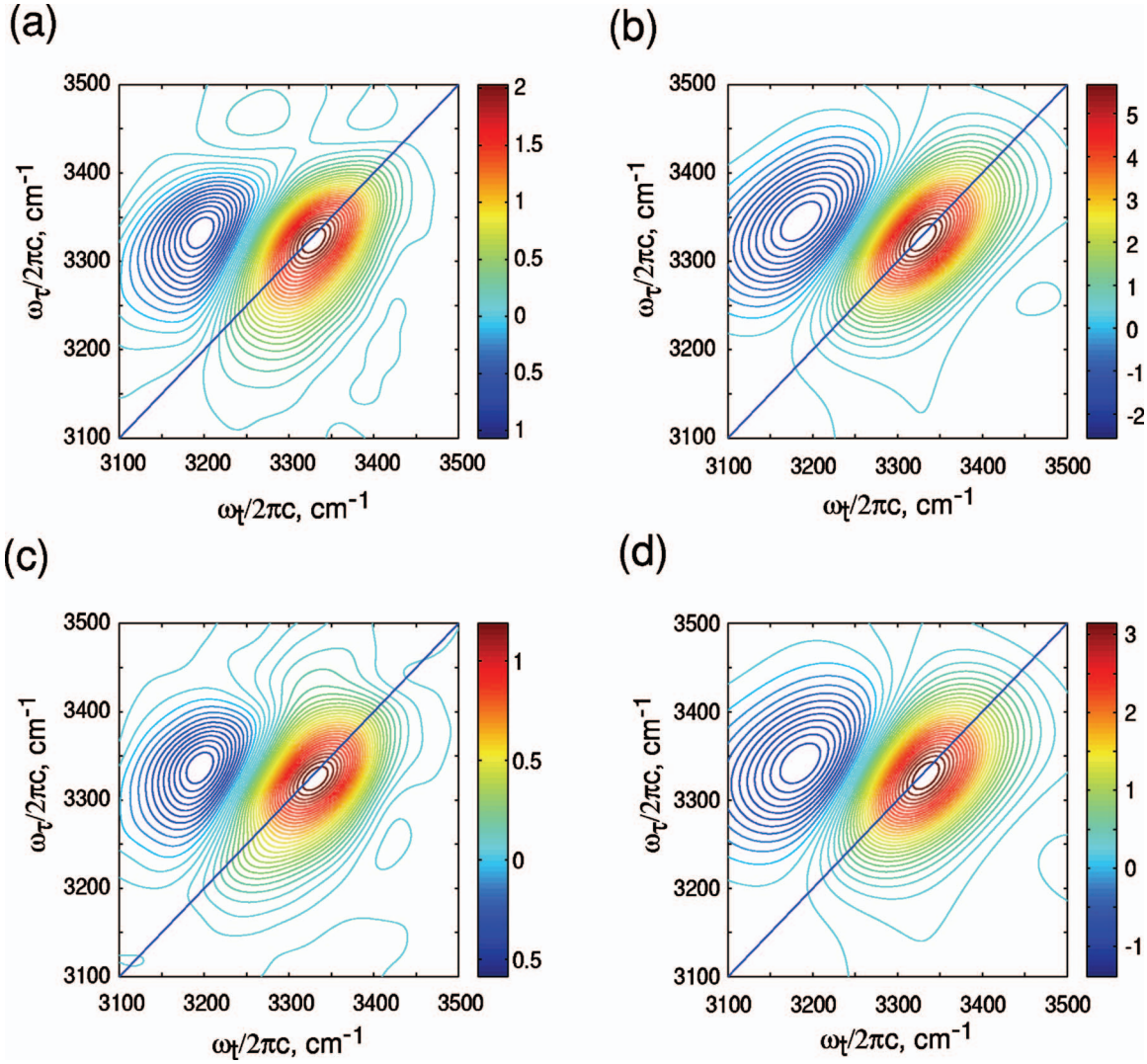

FIG. 4. (Color) The measured (left panel) and simulated (right panel) absorptive 2D IR spectra of the N–H stretching mode of the formamide N–H bond vibration in formamide-D_3 as a function of time T. [(a) and (b)] T=210 fs and [(c) and (d)] T=600 fs.

correspond to the ~95 cm^{-1} mode observed in the Fourier-transformed power spectrum of our experiment. The oscillation in the peak shift demonstrates that the N–H stretch mode oscillation is modulated by the underdamped intermolecular hydrogen-bond motion in the liquid.

The 2D IR spectra are shown in Figs. 4(a) and 4(c). Figure 4(a) corresponds to the 2D spectrum measured at T =0.21 ps and Fig. 4(c) is that at T=0.6 ps. The simulations of these spectra corresponding to the fitting function given above are shown in Figs. 4(b) and 4(d), respectively. The simulated 2D IR spectral shapes show very good agreement with experiment. Two main peaks which correspond to the $0\rightarrow1$ and $1\rightarrow2$ transitions of the N–H stretching mode are observed along the ω_t axis. The diagonal positive peak is the $0\rightarrow1$ transition and the negative peak that is shifted to lower frequency along the ω_t axis by the diagonal anharmonicity is the $1\rightarrow2$ transition. The elongated diagonal peak at T =0.6 ps is elliptically shaped, which implies that the inhomogeneous broadening of the $0\rightarrow1$ transition is persistent until T=0.6 ps. However, as the T values get larger from 0.21 to 0.6 ps, the diagonal peaks become more circular. This effect is the spectral manifestation of the spectral diffusion implied by the correlation function and Eq. (14).

B. DCONH$_2$ in formamide (HCONH$_2$)

The linear IR-absorption spectrum (solid line) of the C–D stretch vibration near 5 μm of $DCONH_2$ in formamide is shown in Fig. 5 with the background absorption from formamide removed. The C–D absorption band (~39 cm^{-1}) is much narrower than that of N–H (~180 cm^{-1}). The peak position is shifted to higher frequency compared with formamide in nonhydroxylic solvents[40] as a result of hydrogen bonding. The IR pulses were centered at the C–D peak position and had sufficient bandwidth to span the fundamental $0\rightarrow1$ and the $1\rightarrow2$ transitions.

The profile of the quantity $|\tilde{S}(\tau,T,\omega_t)|$ vs τ at different values of T were obtained by adding the signals ($|\tilde{S}(\tau,T,\omega_t)|$) over the range of ω_t from 2158 to 2178 cm^{-1}. This procedure samples only the fundamental $0\rightarrow1$ transition of the C–D stretch. As shown in Fig. 6, the peak shift obtained by this procedure decays but shows no oscillation in contrast to

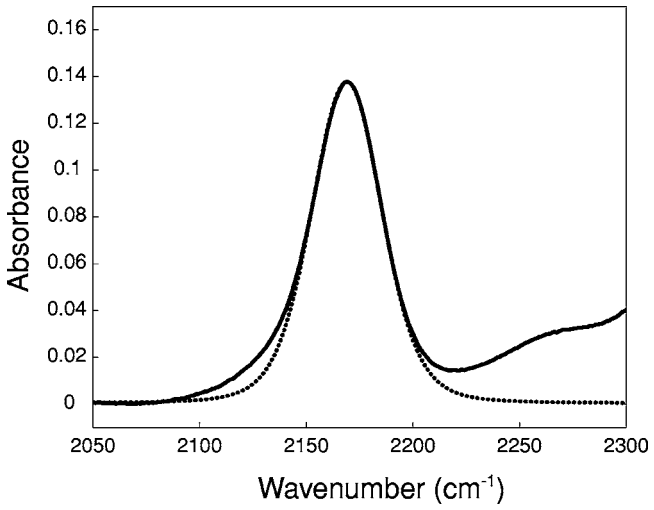

FIG. 5. The linear IR-absorption spectrum (solid line) of the C–D stretch vibration of $DCONH_2$ in formamide-H_3. The dotted line is the spectrum of the linear-response function [Eq. (17)].

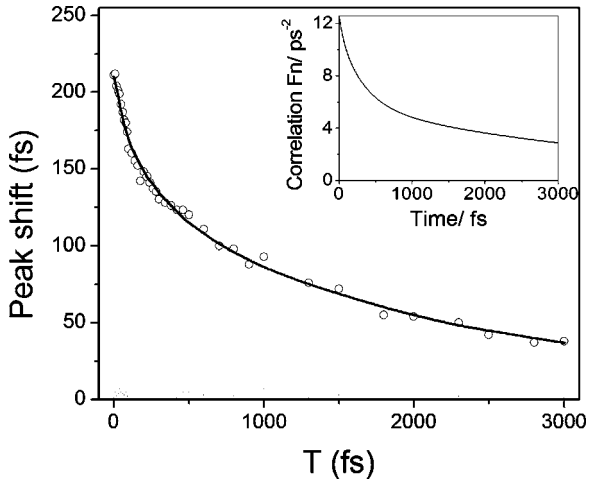

FIG. 6. The measured peak shifts (circle) of the spectrally resolved echo of the C–D stretch vibration as a function of waiting time T. The fitted solid line is the peak shift simulated with the parameters in Table I. The vibrational frequency correlation function is shown in the inset.

the case of the N–H stretch mode. The peak shift of C–D does not show any increase in the picosecond region comparable with that reported for N–H, so the cross correlation pathways involving the $|y\rangle$ states were not included in the analysis. In these simulations, the C–D frequency fluctuations are completely characterized by $\langle x(t)x(0)\rangle$ which is symmetric in x. We assumed that ω_{10} and ω_{21} have strictly correlated fluctuations and the same parameters were used in g_{xx} for both the $\nu=0\rightarrow\nu=1$ and the $\nu=1\rightarrow\nu=2$ transitions. The third-order real three-time electric-field signal was again simulated by convolution of the response functions with the electric fields of the laser pulses [Eq. (15)]. The pulse duration of 80 fs was used in this numerical convolution. The T_1 relaxation time of the C–D vibration was measured to be 1.5 ps from the transient grating experiment, $|\tilde{S}(\tau=0,\omega_t;T)|$ vs T.

The data were fitted by using a frequency correlation function for the C–D mode consisting of three Kubo functions:

$$\langle x(t)x(0)\rangle = a_1^2\exp(-t/t_1) + a_2^2\exp(-t/t_2) + a_3^2\exp(-t/t_3). \quad (18)$$

The linear spectrum, simulated by Fourier transformation of the linear-response function using Eqs. (14) and (17), is shown in Fig. 5. It agrees with experiment near the center frequency of the vibration but there is the slight disagreement at the high- and low-frequency wings. The set of six parameters that best fitted the linear spectrum and the peak shift were found to be $a_1=1.2$ ps^{-1}, $a_2=2.3$ ps^{-1}, $a_3=2.4$ ps^{-1}, $t_1=0.06$ ps, $t_2=0.33$ ps, and $t_3=4.3$ ps. The time constants for the three decay components of the correlation function are somewhat shorter than those of the N–H mode in formamide when it is fitted to three exponentials. The amplitudes representing the distribution of frequencies are also considerably smaller for C–D than N–H (see Table I).

The 2D IR spectra measured at $T=300$ fs and $T=2$ ps are shown in Figs. 7(a) and 7(c), and the simulated 2D IR spectra in Figs. 7(b) and 7(d). The simulated spectral shapes agree well with the experiments. There are two peaks along the ω_t axis corresponding to the $0\rightarrow1$ (the diagonal positive peak) and $1\rightarrow2$ transitions (the negative peak) of the C–D stretching mode. The diagonal anharmonicity is estimated to be 57 cm^{-1} from the fitting. The main peaks in the 2D IR spectrum are somewhat elongated along the diagonal at $T=0.3$ ps, which implies residual inhomogeneous broadening of the $0\rightarrow1$ transition. However, as the T value increases from 0.3 to 2 ps, the diagonal main peaks become nearly circular as a result of the spectral diffusion implied by the parameters of Eq. (18).

C. $H\underline{C}ONH_2$ in bulk formamide

The amide-I IR absorption at 1685 cm^{-1} in liquid formamide has a bandwidth of 45 cm^{-1}, which is narrower than the N–H and wider than the C–D transitions. The peak position

TABLE I. The amplitudes and correlation times of each component in the fitted three exponential data for three IR active modes.

	a_1	τ_1 (ps)	a_2	τ_2 (ps)	a_3	τ_3 (ps)
N–H	10 ps^{-1}	0.15	6.1 ps^{-1}	0.86	9.9 ps^{-1}	11
C–D	1.2 ps^{-1}	0.06	2.3 ps^{-1}	0.33	2.4 ps^{-1}	4.3
C=O[a]	0.004 ps	0.02	0.051 ps	0.75	0.017 ps	11

[a]The amplitudes in this row correspond to peak shifts obtained by fitting the data in Fig. 8 to three exponentials as discussed in the text.

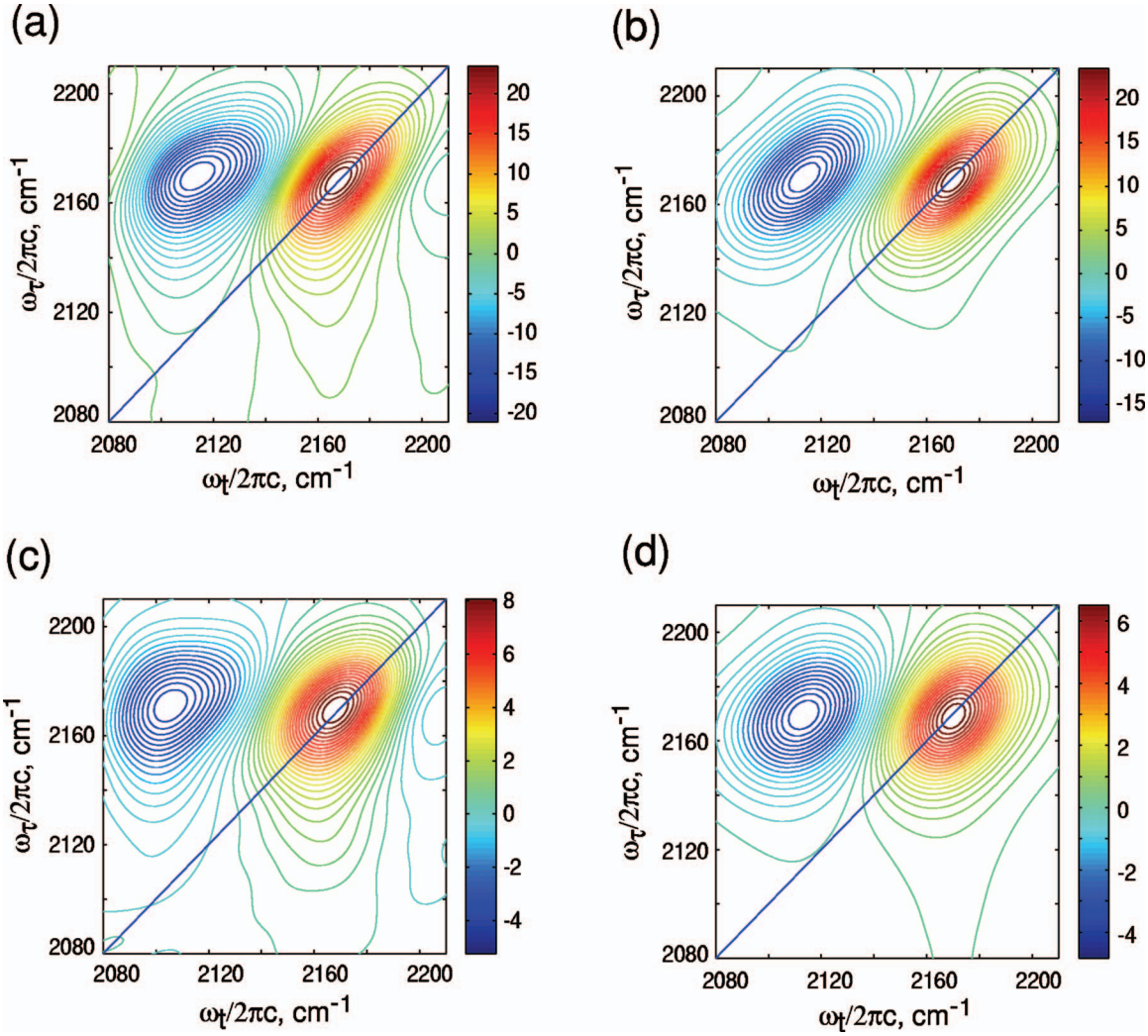

FIG. 7. (Color) The measured absorptive 2D IR spectra (left panel) of the C–D stretching mode of the formamide C–D vibration in formamide-H_3 as a function of time T. The simulated spectra are shown on the right panels. [(a) and (b)] $T=300$ fs and [(c) and (d)] $T=2$ ps.

is shifted to lower frequency by 25 cm^{-1} compared with chloroform (1710 cm^{-1}).[40] Such shifts are typical of H bonding of carbonyls in peptides. The IR pulses used in the nonlinear experiments have sufficient spectral bandwidth to bracket the complete amide-I transition region.

The two-dimensional data were processed to obtain a function $s(\tau,T)$ that is the integral over all t of the absolute magnitude of the complete three-time data set $S(\tau,T,t)$. The function $s(\tau,T)$ resembles the conventional[41] peak shift signal that is the integral over t of the absolute magnitude squared of $S(\tau,T,t)$. The profile of $s(\tau,T)$ is peaked at different τ times depending on the choice of waiting time T. The T dependence of the shift of this peak is plotted in Fig. 8 and reasonably well fitted by three exponentials. The results are summarized in Table I. Note that for C═O the correlation function is not determined by a simulation based on the response functions as was the case for N–H and C–D. Rather, a representation of the frequency correlation function was obtained by direct fitting of the peak shift to a sum of exponentials in the expectation that the parameters obtained would be associated with different physical processes in the liquid. The T_1 relaxation was also measured by processing the same data set to yield $T_1=0.62$ ps.

IV. DISCUSSION

A. Fast dynamics of N–H motion

The correlation functions are described as sums of exponentials, each of which represents a Kubo function. These

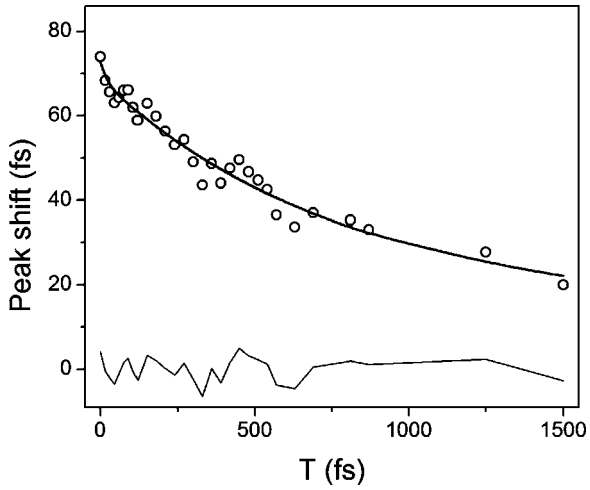

FIG. 8. The measured peak shifts (circle) of the integrated echo and the fit (solid) to three exponential functions. The gray line is the residual of the fit.

functions are not proven to be the actual forms of the correlation decay but represent a convenient way to fit the data to a set of parameters besides suggesting a simple physical interpretation. The reported parameters are a valid representation of the correlation function if the vibrational responses, R_j of Eq. (15), are appropriately defined. Recent works by Skinner and co-workers have drawn attention to the fact that this approach is inappropriate for liquid water.[42,43] We expect that the separated time scales may be associated with different physical processes. The fastest correlation time in the frequency correlation function was measured to be 0.15 ps and its preexponential factor is 10 ps^{-1}, corresponding to a Gaussian width of 125 cm^{-1}, which is slightly smaller than the frequency shift of the N–H stretching mode on forming H bonds to C═O groups. The fastest correlation time corresponds to the modulation of the hydrogen-bond distance and is measured to be close to the fast modulation limit. In the intermediate region below ~1 ps, there are three terms. One is the exponential decay function having the time constant of 860 fs. The other two terms are the sum of the underdamped oscillation terms having the time constants of ~240 fs. In the previous work, the 860 fs correlation time was shown to incorporate only a slight angular motion within a cone angle of 19°. This motion was considered to be related to the overdamped librational motion or hindered rotation around the intermolecular hydrogen bond. This is an angular motion over a space that is much smaller than needed for overall rotation so it is connected with fast angular fluctuations of hydrogen bond. On the other hand, as shown in Fig. 3, the power spectrum of the oscillatory parts (the sum of two underdamped oscillation terms) clearly shows a peak at ~95 cm^{-1}. Other optical spectroscopies such as far-infrared absorption, OHD-RIKES, and depolarized Rayleigh/Raman spectroscopy have indicated that formamide has low-frequency vibrational modes at ~100 and ~190 cm^{-1}.[34–39] The underdamped motion in our experiment most likely corresponds to the ~100 cm^{-1} mode, which was previously assigned as an intermolecular libration of H-bonded formamide molecules. *Ab initio* calculations of formamide clusters assign this frequency to the out-of-plane rotational motion around an axis through the *trans* N–H bond.[44,45] In the echo experiment, the correlation function does not clearly show an ~190 cm^{-1} oscillation. The absence of this mode may be caused by the limited laser-pulse bandwidth (~190 cm^{-1}), but it is possible that the ~190 cm^{-1} librational intermolecular motions do not significantly modulate the N–H stretch coordinate or that the associated form responsible for this mode[37] has a too low concentration in the liquid.

B. Comparison of the frequency correlation functions of the N–H and C–D modes

The frequency correlation functions of the N–H and C–D vibrators yield quite different parameters when fitted to three exponentials (see Table I). In each time regime identified by the fitting, the C–D stretching mode correlation times are faster than those of N–H, indicating the faster spectral diffusion for the C–D stretch band. Since the main source of spectral diffusion is considered to be the movement of the hydrogen-bonded network, this faster correlation decay implies that the environment probed by the C–D mode is considerably more flexible and less tightly coupled than that sensed by the N–H mode.

The frequency correlation functions of the C–D mode do not show underdamped oscillatory components. For the underdamped C–D···O motion to be incorporated effectively into the C–D vibrational transition frequency, there must be a strong correlation between the C–D stretching vibration and the C···O distance (R).[46–49] The *ab initio* molecular-dynamics (MD) simulations predict a broad distribution of C–D···O angles, which is consistent with our measurement.[18] Another reason why oscillatory components are not seen in the frequency correlation function of the C–D vibration could be related to the average angle between the C–D and N–H bonds. The 100 cm^{-1} librational motion originates from the rotational motion in the out-of-plane direction around an axis that is close to the *trans* N–H bond:[44,45] this axis is almost perpendicular to the C–D bond. Therefore, this librational mode may be only weakly coupled to the C–D stretching mode.

The C–D and N–H stretching vibration modes are, in principle, coupled through the intramolecular potential. Therefore, if the N–H bond has low-frequency components due to its coupling to the environment these motions might be expected to show up in other formamide modes that are anharmonically coupled to N–H. We employed density-functional theory (DFT) at the B3LYP/6-31+G^{**} level to examine the modes and mode couplings in formamide using the previously described approach.[50] The potential-energy distribution in the harmonic force field shows that 99% of the C–D stretch normal mode is localized on the C and D atoms. Furthermore, a computation of the diagonal anharmonicity of the C–D mode shows that 69.1 cm^{-1} out of the total 75 cm^{-1} is the intrinsic anharmonicity of the C–D motion. Coupling to the C═O mode contributes 3 cm^{-1}, while coupling to the N–H contributes only 2×10^{-4} cm^{-1} to the C–D anharmonicity. These results strongly suggest that perturbations on the N–H motion by the environment are not likely to be sensed by the C–D bond vibration, which is very strongly isolated from N–H in these computations. Our experiments are consistent with this prediction.

C. Relation of the C–D frequency correlation function to liquid structure and dynamics

The C–D stretch frequency is shifted to higher frequency on hydrogen bonding.[51] This behavior is opposite to that found for N–H and O–H but similar to that found for some ions. A possible explanation[52–54] of such behavior is that the electric field created by the acceptor atom in a hydrogen bond gives rise to a force that tends to lengthen or shorten the $X-H$ bond depending on whether the dipole derivative of the bond is parallel or antiparallel to the field.

The preexponential factor (a_1) of the fastest, motionally narrowed, part of frequency correlation function of the C–D stretch mode is 1.2 ps^{-1}. From this preexponential factor, we can estimate the corresponding inhomogeneous width to be

$a_1\sqrt{\ln 4}/\pi c = 15\ \mathrm{cm}^{-1}$. As in the case of the N–H oscillator, this value is not much smaller than the frequency shift of the C–D stretching mode on forming a hydrogen bond to the C═O group. The C–D frequency for formamide shifts by 21 cm^{-1} between $CHCl_3$ and the neat liquid. With this interpretation of the amplitude, the fast correlation time corresponds to the modulation of H-bond distance. The much smaller frequency shift of the C–D compared with the N–H stretch mode on forming a hydrogen bonding is consistent with the hydrogen-bonding strength of the C–D to C═O being much weaker. On the other hand, the correlation time of the fastest part of the C–D stretch frequency correlation function is faster than that found for N–H and it is in the fast modulation limit.

The rotational relaxation of the N–H bond in liquid formamide is dominated by an 11 ps component.[10] The contributions to the overall dephasing on the ca. 1 ps time scale when angular motions are restricted can be assessed by their relative amplitudes in the frequency correlation function. The intermediate time scale contributes 39% to the $t=0$ amplitude of the C–D frequency correlation function but only 23% to that of the N–H stretch mode. The spectral diffusion is faster and more extensive for C–D than for N–H during this intermediate time scale when the overall motions are strongly restricted. We conclude that the changes in liquid state structure in the immediate vicinity of the C–D bond are more significant than those around N–H, consistent with there being fewer C–D hydrogen bonds.[18] In the case of the N–H bond, the ca. 1 ps motions were considered to mediate the vibrational relaxation by fluctuating the force exerted on the N–H bond.[10] However, for the C–D bond, the T_1 relaxation time is 1.5 ps, which is much slower than the correlation time of the intermediate time scale component. It is suggested that the weak hydrogen bonding of C–D generates significantly smaller forces than exerted on N–H by carbonyl groups.

The slowest frequency correlation component of the N–H bond was assigned as the breaking and making of the hydrogen-bonded structure. For the C–D stretching vibration motion, the slowest frequency correlation time is 4.3 ps, which is one-third of the time found for the N–H bond. Clearly the making and breaking dynamics of the C–D hydrogen bond is much more rapid than that of N–H.

The positive diagonal signals (the fundamental $0\rightarrow 1$ transitions) of the experimental 2D IR spectra of C–D agree well with the simulations at $T=300$ fs, indicating that the distribution of frequency fluctuations of C–D is almost Gaussian during this early period (see Fig. 7). However, at $T=2$ ps the high-frequency part of the 2D IR spectrum has a narrower bandwidth than seen in the simulated spectrum. This effect suggests that the relaxation rates are slightly frequency dependent. The high-frequency part of the C–D vibrational spectrum corresponds to the more hydrogen-bonded species, for which the spectral diffusion process may be slower than that of the more free species that dominate the low-frequency edge of the band. Another possible reason for the variations in shape could be the frequency dependence of the transition dipole moment.[42,43] However, we have shown that the transition dipole for C–D is the same within 10% for formamide not H bonded (in $CHCl_3$) and H bonded in formamide liquid.

D. Vibrational dynamics of amide-I mode in bulk formamide

For the amide-I transition the response functions are expected to be more complicated than those for a single oscillator, since it is obvious from the 2D IR spectra and linear IR spectra that there is significant mode coupling between different molecules.[55–57] However, the decay of the echo peak shift is expected to yield a qualitative representation of the frequency correlation function. We note that these amide-I experiments were not fitted to simulations using the response functions as in the N–H and C–D examples. The amide-I peak shift data were directly fitted to a sum of three exponentials. The most slowly varying part of the C═O peak shift data corresponds approximately to the same structure breaking time that was observed for the N–H mode and is consistent with the orientational dynamics of the N–H bond (see Table I). Furthermore, an intermediate time scale of ca. 1 ps is observed for both N–H and C═O. During this 1 ps period the orientational order is largely maintained and so hydrogen-bond fluctuations within a given set of structures are the most obvious interpretation.

The fastest part of amide-I frequency correlation function makes only a small contribution to the peak shift profile suggesting that the relevant distribution is motionally narrowed. We know from fitting to the response functions that motionally narrowed contributions have a small influence on the correlation function. The intermediate time scale process has a peak shift of ~10 fs for N–H. From the fact that the peak shift is inversely related to amplitude factor in the correlation function,[58] it can be concluded that the distribution of N–H frequency fluctuations corresponding to the intermediate time scale is about five times wider than for C═O. These relative magnitudes track the spectral shifts on hydrogen bonding of C═O (30 cm^{-1}) and N–H (150 cm^{-1}). The correlation times of the intermediate process are very similar for C═O (0.75 ps) and N–H (0.86 ps), suggesting that the same H-bond dynamics are involved in the spectral diffusion of both modes. The C–D bond peak shift does not exhibit this 0.8 ps process, showing clearly that it is located in an environment that dephases the mode more rapidly (0.3 ps). However, the intermediate time scale (0.3 ps) is still dominant in the peak shift decay of C–D suggesting that C–D is also involved in hydrogen-bonding interactions.

V. CONCLUSION

The vibrational frequency correlation function of the C–D stretch mode decays in three time regimes ascribed to the modulation of the H-bond distance, the overdamped libration of the intermolecular hydrogen bond, and the overall structure breaking and making. The correlation times for the C–D stretch mode obtained by fitting to three exponentials are faster than those of the N–H mode, implying that the liquid structure around the C–D bond is less rigid and the related motions of the C–D bond are relatively faster than

that of N–H. Underdamped oscillatory behavior having the character of the low-frequency hydrogen-bond intermolecular librational motion was apparent only for the N–H stretch mode. In the case of the amide-I (carbonyl) mode, the frequency distribution of the fastest component is motionally narrowed and the intermediate and slow components have similar characteristic time constants to those of N–H, indicating that they are both caused by the strong intermolecular hydrogen-bonding interaction. Liquid formamide is envisaged as a N–H···O=C hydrogen-bond network, reinforced by the weaker C–H···O=C hydrogen bonds. The conformational changes around the C–H bond are the most facile. These structural conclusions are consistent with recent *ab initio* dynamics calculation.[18]

ACKNOWLEDGMENTS

This research was supported by grants from NSF (CHE) and NIH (GM12592) with instrumentation from NIH Resource Grant No. RR01348. We gratefully acknowledge assistance from J. Wang for the DFT analysis.[50]

[1] P. Hamm and R. M. Hochstrasser, in *Ultrafast Infrared and Raman Spectroscopy*, edited by M. D. Fayer (Dekker, New York, 2001), p. 273.
[2] M. T. Zanni, N.-H. Ge, Y. S. Kim, and R. M. Hochstrasser, Proc. Natl. Acad. Sci. U.S.A. **98**, 11265 (2001).
[3] M. T. Zanni, S. Gnanakaran, J. Stenger, and R. M. Hochstrasser, J. Phys. Chem. B **105**, 6520 (2001).
[4] M. C. Asplund, M. T. Zanni, and R. M. Hochstrasser, Proc. Natl. Acad. Sci. U.S.A. **97**, 8219 (2000).
[5] Y. S. Kim and R. M. Hochstrasser, J. Phys. Chem. B **109**, 6884 (2005).
[6] C. Fang, J. Wang, Y. S. Kim, A. K. Charnley, W. Barber-Armstrong, A. B. Smith III, S. M. Decatur, and R. M. Hochstrasser, J. Phys. Chem. B **108**, 10415 (2004).
[7] H. S. Chung, M. Khalil, A. W. Smith, Z. Ganim, and A. Tokmakoff, Proc. Natl. Acad. Sci. U.S.A. **102**, 612 (2005).
[8] N.-H. Ge, M. T. Zanni, and R. M. Hochstrasser, in *Ultrafast Phenomena XIII*, edited by R. D. Miller, M. M. Murnane, N. F. Scherer, and A. M. Weiner (Springer-Verlag, Berlin, 2003), p. 592.
[9] M. L. Cowan, B. D. Bruner, N. Huse, J. R. Dwyer, B. Chugh, E. T. J. Nibbering, T. Elsaesser, and R. J. D. Miller, Nature (London) **434**, 199 (2005).
[10] J. Park, J.-H. Ha, and R. M. Hochstrasser, J. Chem. Phys. **121**, 7281 (2004).
[11] J. B. Asbury, T. Steinel, and M. D. Fayer, J. Phys. Chem. B **108**, 6544 (2004).
[12] J. B. Asbury, T. Steinel, C. Stromberg, S. A. Corcelli, C. P. Lawrence, J. L. Skinner, and M. D. Fayer, J. Phys. Chem. A **108**, 1107 (2004).
[13] J. T. Fourkas, Annu. Rev. Phys. Chem. **53**, 17 (2002).
[14] A. C. Gomez Marigliano and E. L. Varetti, J. Phys. Chem. A **106**, 1100 (2002).
[15] P. G. Puranik and K. V. Ramiah, J. Mol. Spectrosc. **3**, 486 (1959).
[16] Y. P. Puhovski and B. M. Rode, Chem. Phys. **190**, 61 (1995).
[17] Y. P. Puhovski, L. P. Safonova, and B. M. Rode, J. Mol. Liq. **103–104**, 15 (2003).
[18] E. Tsuchida, J. Chem. Phys. **121**, 4740 (2004).
[19] G. A. Jeffrey, *An Introduction to Hydrogen Bonding* (Oxford University Press, New York, 1997).
[20] J. K. Chin, R. Jimenez, and F. E. Romesberg, J. Am. Chem. Soc. **123**, 2426 (2001).
[21] J. K. Chin, R. Jimenez, and F. E. Romesberg, J. Am. Chem. Soc. **124**, 1846 (2002).
[22] L. Bu and J. E. Straub, Biophys. J. **85**, 1429 (2003).
[23] L. B. Sagle, J. Zimmermann, P. E. Dawson, and F. E. Romesberg, J. Am. Chem. Soc. **126**, 3384 (2004).
[24] A. Allerhand and P. v. R. Schleyer, J. Am. Chem. Soc. **85**, 1715 (1963).
[25] G. R. Desiraju, Acc. Chem. Res. **24**, 290 (1991).
[26] J. Bella and H. M. Berman, J. Mol. Biol. **264**, 734 (1996).
[27] R. Vargas, J. Garza, D. A. Dixon, and B. P. Hay, J. Am. Chem. Soc. **122**, 4750 (2000).
[28] R. Vargas, J. Garza, R. A. Friesner, H. Stern, B. P. Hay, and D. A. Dixon, J. Phys. Chem. A **105**, 4963 (2001).
[29] A. Senes, I. Ubarretxena-Belandia, and D. M. Engelman, Proc. Natl. Acad. Sci. U.S.A. **98**, 9056 (2001).
[30] B. Loll, G. Raszewski, W. Saenger, and J. Biesiadka, J. Mol. Biol. **328**, 737 (2003).
[31] A. Mortensen, O. F. Nielsen, J. Yarwood, and V. Shelley, J. Phys. Chem. **98**, 5221 (1994).
[32] A. Mortensen, O. F. Nielsen, J. Yarwood, and V. Shelley, J. Phys. Chem. **99**, 4435 (1995).
[33] J. Chen, J. Park, and R. M. Hochstrasser, J. Phys. Chem. A **107**, 10660 (2003).
[34] K. Itoh and T. Shimanouchi, J. Mol. Spectrosc. **42**, 86 (1972).
[35] Y. J. Chang and E. W. Castner, Jr., J. Chem. Phys. **99**, 113 (1993).
[36] Y. J. Chang and E. W. Castner, Jr., *Sixth International Conference on Time-Resolved Vibrational Spectroscopy*, edited by A. Lau, F. Siebert, and W. Werncke (Springer-Verlag, Berlin, 1994), p. 145.
[37] Y. J. Chang and E. W. Castner, Jr., J. Phys. Chem. **98**, 9712 (1994).
[38] O. F. Nielsen and P. A. Lund, Chem. Phys. Lett. **78**, 626 (1981).
[39] O. F. Nielsen, P. A. Lund, and E. Praestgaard, J. Chem. Phys. **77**, 3878 (1982).
[40] Y. Tanaka and K. Machida, J. Mol. Spectrosc. **63**, 306 (1976).
[41] T. Joo, Y. Jia, J.-Y. Yu, M. J. Lang, and G. R. Fleming, J. Chem. Phys. **104**, 6089 (1996).
[42] S. A. Corcelli and J. L. Skinner, J. Phys. Chem. A **109**, 6154 (2005).
[43] J. R. Schmidt, S. A. Corcelli, and J. L. Skinner, J. Chem. Phys. **123**, 044513/1 (2005).
[44] H. Torii and M. Tasumi, Int. J. Quantum Chem. **70**, 241 (1998).
[45] H. Torii and M. Tasumi, J. Phys. Chem. A **104**, 4174 (2000).
[46] R. Rey, K. B. Moller, and J. T. Hynes, J. Phys. Chem. A **106**, 11993 (2002).
[47] K. B. Moller, R. Rey, and J. T. Hynes, J. Phys. Chem. A **108**, 1275 (2004).
[48] C. P. Lawrence and J. L. Skinner, J. Chem. Phys. **118**, 264 (2003).
[49] C. J. Fecko, J. J. Loparo, S. T. Roberts, and A. Tokmakoff, J. Chem. Phys. **122**, 054506 (2005).
[50] J. Wang and R. M. Hochstrasser, "Anharmonicity of amine modes," J. Phys. Chem. B, published online 23 August 2005 (DOI: 10.1021/jp0530092).
[51] P. Hobza and Z. Havlas, Chem. Rev. (Washington, D.C.) **100**, 4253 (2000).
[52] W. Qian and S. Krimm, J. Phys. Chem. A **106**, 11663 (2002).
[53] W. Qian and S. Krimm, J. Phys. Chem. A **106**, 6628 (2002).
[54] N. G. Mirkin and S. Krimm, J. Phys. Chem. A **108**, 5438 (2004).
[55] H. Torii and M. Tasumi, J. Phys. Chem. B **102**, 315 (1998).
[56] H. Torii, J. Phys. Chem. A **106**, 3281 (2002).
[57] H. Torii, J. Phys. Chem. A **108**, 2103 (2004).
[58] K. F. Everitt, E. Geva, and J. L. Skinner, J. Chem. Phys. **114**, 1326 (2001).